

Near surface structure of Sodankylä area in Finland, obtained by ~~advanced method of~~ passive seismic interferometry

Nikita Afonin^{1,5}, Elena Kozlovskaya^{1,2,4}, Suvi Heinonen², Stefan Buske³

¹Oulu Mining School, POB-3000, FIN-90014, University of Oulu, Finland

²Geological Survey of Finland, P.O. Box 96, FI-02151, Espoo, Finland

³TU Bergakademie Freiberg, Institute of Geophysics and Geoinformatics, Freiberg, Germany

⁴Sodankylä Geophysical Observatory, University of Oulu, Finland

⁵N. Laverov Federal Center for Integrated Arctic Research of the Ural Branch of the Russian Academy of Sciences, Arkhangelsk, Russia

Correspondence to: Nikita Afonin (nikita.afonin@oulu.fi)

Abstract. Controlled-source seismic exploration surveys are not always possible in nature-protected areas. As an alternative, application of passive seismic techniques in such areas can be proposed. In our study, we show results of passive seismic interferometry application for mapping the uppermost crust in the area of active mineral exploration in Northern Finland. We are utilizing continuous seismic data acquired by Sercel Unite Wireless multichannel recording system along several profiles during XSoDEx (eXperiment of SOdankylä Deep Exploration) [multidisciplinary geophysical project](#).—The objective of [XSoDEx the project](#) was to obtain a structural image of the upper crust in the Sodankylä area of Northern Finland in order to achieve a better understanding of the mineral system at depth. The key experiment of the project was a high-resolution seismic reflection experiment, and continuous passive seismic data was acquired in parallel with reflection seismic data acquisition. Due to this, the length of passive data suitable for noise cross-correlation was limited ~~to from~~ several hours [to couple of days](#). In addition, analysis of the passive data demonstrated that dominating sources of ambient noise are non-stationary and have different origin across the XSoDEx study area. As the long data registration period and isotropic azimuthal distribution of noise sources are two major conditions for diffuse wavefield necessary for Empirical Green’s Functions (EGFs) extraction, [it was not possible to apply](#) the conventional techniques of passive seismic interferometry ~~was not possible to apply~~. To find the way to obtain EGFs, we used numerical modelling to investigate the properties of seismic noise originating from sources with different characteristics and propagating inside synthetic heterogeneous Earth models that models real geological conditions in the XSodEx study area. The modelling demonstrated that scattering of ballistic waves on irregular shape heterogeneities, such as massive sulphides or mafic intrusions, could produce diffused wavefield composed mainly of scattered surface waves. This scattered wavefield can be used to retrieve reliable Empirical Green Functions (EGFs) from short-term and non-stationary data, using a special technique called “signal-to-noise ratio stacking” (SNRS). The EGFs calculated for the XSoDEx profiles were inverted in order to obtain S-wave velocity models down to the depth of 300 meters. The obtained velocity models agree well with geological data and complement the results of reflection seismic data interpretation.

Formatted: English (United Kingdom)

Formatted: English (United Kingdom)

1 Introduction

Exploration of new mineral deposits is an actual task because the modern world needs many types of minerals for functioning (Reid, 2011). Most of the shallow mineral deposits around the world nowadays are well known and exploration of new deep mineral deposits becomes more difficult than earlier (Vasara, 2018). That is why the cost-effectiveness of exploration also decrease. Moreover, there is the problem that application of controlled-source seismic exploration is not always possible in nature-protected areas. Particularly in the Arctic areas, non-invasive, environmentally friendly exploration is relevant. As an alternative, application of passive seismic techniques in such areas has been proposed. The main advantage of passive seismic methods is possibility to study the subsurface in remote areas with minimum impact to environment (Polychronopoulou et al., 2020).

Passive seismic interferometry is cost-efficient methodology with relatively simple setup of field experiments. This methodology allows retrieving impulse response of a medium (Empirical Green's Function) from ambient seismic noise recorded at two receivers, assumed that the noise field is diffuse (Lobkis and Weaver, 2001; Campillo and Paul, 2003). If this condition is satisfied, it is possible to retrieve both surface and body waves from seismic noise by passive seismic interferometry based on either crosscorrelation, autocorrelation, deconvolution or cross-coherence of seismic records (Wapenaar et al., 2011). As shown in (Ricker and Claerbout, 1999) the condition of diffuse noise field is satisfied if the noise sources are distributed isotopically around seismic recorders and the noise registration time is long enough. The methodology to retrieve empirical Greens functions, using crosscorrelation or autocorrelation of ambient seismic noise, has been successfully applied in numerous studies (e.g. Shapiro and Campillo, 2004; Roux et al., 2005; Ruigrok et al., 2011; Draganov et al., 2009; Poli et al., 2012; Tibuleac et al., 2012; Wang et al., 2015; Taylor et al., 2016; Afonin et al., 2017; Oren and Nowack, 2016; Romero et al., 2018). In addition to ambient seismic noise interferometry, the coda wave interferometry was proposed (Aki and Richards, 2002; Campillo et al., 2003; Snieder et al., 2002; Snieder, 2006). This methodology is also based on diffuse field approximation and it is widely used for different purposes, such as estimating nonlinear behavior in seismic velocity (Snieder et al., 2002), monitoring of stress changes inside the studied medium (Grêt et al., 2005, 2006) and determination of third order elastic constants in a complex solid (Payan et al., 2009). Numerous studies describe results of successful application of passive seismic interferometry for exploration and other applied geophysical purposes (e.g. Cheraghi et al., 2017; Roots et al., 2017; Dantas et al., 2018; Abraham et al., 2019; Polychronopoulou et al., 2020; Planès et al., 2020).

In spite of these numerous studies, there is the problem that the conditions of diffuse noise field from sources outside observation area are difficult to satisfy in many practical situations. These conditions are isotropic (that is, when waves arrived from all azimuths) and homogeneous (when the waves arrived from all azimuths have near the same energy) azimuthal distribution of noise sources and long registration time. However, the diffuse wavefield for empirical Green's functions evaluation can exist also under other conditions. Wapenaar (2004) demonstrated that empirical Green functions could be retrieved from cross correlation of two recordings of a wavefield at different receiver locations at the free surface in the case when diffuse wavefield is produced by many uncorrelated sources inside the medium. Wapenaar and Thorbecke (2013) also

Formatted: English (United Kingdom)

Formatted: English (United Kingdom)

Formatted: English (United Kingdom)

Formatted: English (United Kingdom)

considered conditions for empirical Green's function retrieval from ambient noise from a directional scatterer in a homogeneous embedding medium, illuminated by a directional noise field.

In our paper, we examine application of passive seismic interferometry for the case when noise is strongly directional and receiver array is semi-linear. For this, we use continuous seismic data recorded during XSoDEx (eXperiment of SOdankylä Deep Exploration) project in northern Finland (Buske et al., 2019). We analyze the ambient seismic noise recorded by stations located in different sub-regions of the XSoDEx study area in order to understand spatial and temporal distribution of noise sources. We perform numerical modelling of propagation of signals corresponding to identified noise sources through various synthetic models, representing certain types of heterogeneities (massive sulfides, mafic intrusions, faults). We show by numerical modelling that direct waves, generated by various sources are scattered on these heterogeneities and produce diffused wavefield. Therefore, empirical Greens function ~~of the studied medium~~ can be retrieved by crosscorrelation of this wavefield recorded at different locations (Wapenaar, 2004; Wapenaar and Thorbecke, 2013; van Manen et al., 2005). For evaluation of empirical Greens functions, we apply advanced method of passive seismic interferometry (Afonin et al., 2019) that we called signal-to-noise ratio stacking (SNRS). We show results of application of passive seismic interferometry for mapping the uppermost crust in the area of XSoDEx project.


Formatted: English (United Kingdom)

Formatted: English (United Kingdom)

2 Experiment description

The XSoDEx seismic survey was conducted in the Central Lapland Greenstone belt in Northern Finland, around Sodankylä region (Figure 1). Area is famous for its mineral deposits ~~and active exploration~~, including operating Kittilä Gold mine west from the survey area and Kevitsa Ni-Cu mine that also has significant amounts of platinum, palladium, gold and cobalt. The seismic survey lines are crossing varying geology including outcrops of Archean basement and layered mafic intrusions (Buske et al., 2019).

Formatted: English (United Kingdom)

Within XSoDEx project, Geological Survey of Finland, TU Bergakademie Freiberg and University of Oulu acquired seismic reflection and refraction data using the Vibroseis  truck of TU Bergakademie Freiberg ~~and partly explosive sources~~ during July and August 2017 resulting in four seismic profiles of total length of approximately 80 km (figure 1): Pomokarantie line (about 37.5 km); Alaliesintie line (about 14 km); Saakatti line (about 20 km); Kuusivaarantie line (about 16 km). The seismic reflection data were recorded in a roll-along scheme by a maximum 3.6 km long spread of cabled vertical-component geophones with 10 m spacing. The seismic reflection layout was designed to map crustal structures down to a minimum of 3 km depth in detail. The seismic refraction data were recorded along all reflection profiles by 60 vertical component 5 Hz geophones and 40 three-component MEMS accelerometers with SerCEL Unite SerCEL Ltd wireless autonomous data acquisition units by SerCEL Ltd. MEMS accelerometers along an extended line around the reflection spread with maximum offsets of around 10 km. These ~~instrument sensors~~ were installed with interstation distances of 160 m, ~~and with maximum offsets of around about 10 km~~, between each other and recorded continuous seismic data with the sampling frequency of 500 Hz ~~every day since about 07:00 to about 22:00 GMT~~. Refraction seismic data was extracted from the continuous data during periods when active seismic source was in operation, while the passive seismic data were accumulated during periods when active

Formatted: English (United Kingdom)

100 seismic source was not working (night time, spare days). Thus, the XSoDEx experiment provided a good opportunity to verify results of passive seismic interferometry with controlled-source seismic data, to identify limitations of this technique in areas of generally low level of high-frequency anthropogenic noise and to propose possible improvements of known techniques.

3 Ambient seismic noise in XSoDEx study area

105 In addition toIn additional to microseismic noise, there are several local noise sources in the XSoDEx study area. They are industrial noise from Kevitsa Mine, traffic noise from the roads and noise from water-power plants of Kitinen River. For estimation and comparison of noise level for different XSoDEx profiles, we used vertical components of ambient seismic noise recorded by wireless seismic stations. The datawireless-data was not acquired during nighttime on Sundays, when anthropogenic activity is minimal. As one can see in Figure 2, the noise amplitude-level and its frequency spectra differ significantly at stations located atat different sites in XSoDEx area-profiles.

110 The station V1 was installed in the area characterized by the highest noise level for all-analyzed-frequencies analyzed. It can be explainedIt is likely-caused by location of this station close to the Kevitsa mine and the dam of a waterpower plant. Seismic noise recorded by station P2 was hascharacterized-by the lower amplitudelevel, than the seismic-noise recorded by V1 station. It can be suggested that-Probably the main noise sources at that station were a road and the dam. A narrow peak at frequencies of about 26-30 Hz is seencharacterizes in the seismic noise spectrum ofat station V2. We suggest that the main noise source at the V2 was the dam. Unexpected results of noise level estimations were obtained for stations P2 and A. As one can see in Figure 2, station P2 is characterized by relatively high level of seismic noise. At the same time, seismic noise at station-point A is relatively low, despite similar distance from these stations to the dam and to the road. We need to remember, however, that data acquisition along different profiles was made during different time periods, so probably someone additional high-frequency noise source was acting at P2 during the data acquisition period.

120 It is clear that dominating noise sources are different across thein-various areas of our study, and general condition for passive seismic interferometry (the sources need to be isotopically and homogeneously distributed around the study area) is not satisfied. However, local sources of high intensity can be used for evaluation of EGF for selected profiles. According to Aecording to the results of spectral analysis and la-priori knowledge about locations of potential noise sources, we proposed the followingnext possible candidates for sources of signals for passive seismic interferometry can be proposed:

- 125 1) Kevitsa mine, because all the profiles are located at distances of about 6 – 42 km from the mine;
2) Kitinen River and waterpower plants located on the river, because three of four profiles#nes are located along the river; and water-power plants, because of three dams located along the river;
3) The waves that are scattered on heterogeneities and can produce diffused wavefield, as proposed by van Manen et. al. (2005), Wapenaar (2004), Wapenaar et. al. (2015);
130 4) We can also use the signals from Vibroseis @-vibrosource and explosionsblasts recorded in XSoDEx refraction experiment, in order to utilize propagation of surface waves to long offsets. Such analysis is not possible Normally Due to, i-with the data

Formatted: English (United Kingdom)

Formatted: English (United Kingdom)

Formatted: English (United Kingdom)

Formatted: English (United Kingdom)

Formatted: English (United Kingdom)

Formatted: English (United Kingdom)

Formatted: English (United Kingdom)

Formatted: English (United Kingdom)

Formatted: English (United Kingdom)

Formatted: English (United Kingdom)

Formatted: English (United Kingdom)

Formatted: English (United Kingdom)

135 acquired in a typical near-vertical reflection experiments, because only short offsets and limited recording times are ~~can be~~ used. In addition, active ~~and sources have relatively high frequencies and; using of they can be used~~ surface waves only for shallow subsurface ~~, produced by these sources as is, allowed investigation in and only shallow depth investigated.~~ Nevertheless, scattering of these waves on heterogeneities in the medium may produce diffused wavefield, which could be analyzed by passive seismic interferometry method.

In the next chapter, we investigate the wavefield produced by these possible sources using numerical modelling.

4 Numerical modelling of seismic wavefield from different sources

140 There is a number of previous theoretical and numerical studies of the wavefield from various sources scattered on heterogeneities (Aki, 1969; Wu and Aki, 1985; Frankel and Clayton, 1986; Gritto et al., 1995; Bohlen et al., 2003 etc.). They showed that the scattered wavefield can be quite complicated, depending on the shape of heterogeneity and its elastic properties, location of the receiver in the far field or near field and other factors. For simulation of seismic wavefield propagation in the bedrock typical for XSoDEx area, we used SOFI3D software, which solves a wave equation by finite-difference method (<https://git.scc.kit.edu/GPIAG-Software/SOFI3D/tree/Release>). For simulation of the wavefield scattered on heterogeneities wavefield we developed synthetic model based on *a-priori* knowledge about geological structure of the study area (Leväniemi et al., 2018). We used background velocities of $V_p=5600$ m/s, $V_s=3500$ m/s and density= 2650 kg/m³ corresponding to felsic rocks. The embedded vertical high velocity bodies were representing mafic dykes of 30-150 m wide with depths varying randomly from 60 m to 600 m with the following physical properties (Figure 3): $V_p=6500$ m/s, $V_s=3700$ m/s, density 2800 kg/m³. We also assumed an uppermost 60 m thick layers representing quaternary sediments with $V_p=2000$ m/s, $V_s=1200$ m/s and density 1600 kg/m³. The following elastic properties of air were used as boundary conditions of the model: $V_p=330$ m/s, $V_s=0$, density = 1.25 kg/m³. As sources, we used: 1) plane waves from sources located out of line in far field area, with frequencies of 50 Hz and 2.5 Hz with an incidence angle of 45 degrees; 2) blast with dominant frequency of 30 Hz, located in the beginning of the profile; 3) water power plant (stationary noise with frequency of 2.5 Hz), located in-line with the profile and out of line plane waves with frequencies of 50 Hz and 2.5 Hz arrived with angle of approach of 45 degrees. The assumption about major sources was made based on analysis of spectra, presented in the Section 3, and knowledge about locations of industrial objects, roads and other objects of human activities (Figure 2). In the modelling, we used the grid size of 30 m.

160 The first synthetic signal was a plane wave originating from a source in the far-field area. The wave front propagated from the depth of 6000 m with an azimuth of approach of 40 degrees with respect to the profile direction and arrived at the surface at incidence angle of 45 degrees. As one can see on synthetic seismogram in Figure 4, the recorded wavefield consists of the first arrival, several reflected waves and numerous scattered waves with apparent velocities of 2100-2500 m/s corresponding to surface waves. Figure 5 shows an example of particle motion diagrams (Figure 5, c) and results of spectral analysis of these arrivals (Figure 5, b). Due to elliptical polarization and dependence of phase velocity on frequency, one can conclude, that these waves are surface Rayleigh waves. As these surface waves have stochastic directivities,

Formatted: Superscript

Formatted: Superscript

Formatted: Superscript

Formatted: Superscript

Formatted: English (United Kingdom)

Formatted: English (United Kingdom)

165 superposition of them may be considered as diffused wavefield that can be used, in principle, to estimate Empirical Greens functions.

In this synthetic example, we demonstrate that the diffuse wavefield consisting of low-frequency (5-20 Hz) surface waves (Rayleigh) can be produced by scattering of a high-frequency (50 dozen Hz in our case) plane wave at velocity heterogeneities. We considered monochromatic plane wave, but in real in ambient noise, many frequencies present and scattering would be more pronounced.

170 The second example simulate propagation of the signal originating from production blast in the Kevitsa mine. Figure 6 shows results of modelling of the wavefield produced by the blast and propagating in the model with stochastically distributed heterogeneities. As seen, the wavefield consists of only direct P-wave arrival, reflected P-wave, multiples of P-waves, reflected from vertical heterogeneities, and surface Love wave. In that case, surface Rayleigh waves are absent from the wavefield.

175 The third synthetic example corresponds to the direct wave continuously produced by waterpower plant, which could also be scattered on heterogeneities and produce diffused wavefield. ~~As~~Due to the positions of all of the dams on the Kitinen river are well known in our experiment and all of them are located in-line with the Sakatti profile, we used the in-line position of the source in our simulation synthetic model. As an input signal for simulation, we used a real seismic signal ismogram recorded by station V1 that, which was located at the shortest distance from the waterpower plant (Figure 2). The spectral-time diagram of the signal is presented in Figure 7. As one can see, there are several spectral peaks with frequencies of about 5 Hz, 12.5 Hz and 20-50 Hz. According to (Antonovskaya et al., 2017; 2019), seismic noise generated by waterpower plants may correspond to a set of spectral peaks between 3.6 Hz and about 50 Hz. The oOther spectral peaks could be due to production activities (transportation, excavation etc.) at Kevitsa mine. Therefore, in this case we have complex contribution of all sources to the noise wavefield.

185 Figure 8 (a) shows synthetic seismograms of stationary wavefield produced by the signal cossesponding to spectrogram of which is presented in Figure 7. Analysis of particle motion (Figure 8 (c)) shows that this stationary field is consisting of Rayleigh waves with apparent velocities of about 2100-2500 m/s. Figure 8(b) shows crosscorrelations of the first trace with all other traces in Fig. 8(a). As seen, the wavefield contains also P and S waves.

190 Results of our synthetic modeling demonstrate that the plane wave scattered at heterogeneities satisfies condition of diffuse wavefield and hence can be used to extract EGFs. The wavefield, produced by scattering of stationary signal from the waterpower plant can also be used in the cases when receivers are deployed within the first Fresnel volume area. Usage of the diffuse wavefield produced by scattering on local heterogeneities or stationary wavefield from a single source will have an advantage that in both cases the long registration time necessary for obtaining isotropic azimuthal coverage of ambient noise sources is not required. However, special analysis of the continuous data would be necessary, in order to extract the diffuse wavefield from the data. For this purpose, the SNRS algorithm described earlier in Afonin et al. (2019) can be used. The technique is based on the global optimization algorithm, in which the optimized objective function is a signal-to-noise ratio of an EGF, retrieved at each iteration. Maximizing the signal-to-noise ratio of the retrieved EGF is ensured by stacking only cross- correlation functions coherent with each other and corresponding to the stationary phase area. The main idea of this

Formatted: English (United Kingdom)

Formatted: English (United Kingdom)

Formatted: English (United Kingdom)

Formatted: English (United Kingdom)

Formatted: English (United Kingdom)

algorithm is selecting from the wavefield only those waves, which arrive from near-zero azimuths of approaches and stacking them to obtaining empirical Green's functions with a high signal-to-noise ratio. The selection is based on a global optimization algorithm, where a-priori assumptions about seismic velocities in the studied medium are used as a starting model.

5 Verifying passive seismic interferometry with the scattered diffuse wavefield using with passive seismic data recorded during XSoDEx experiment

In order to demonstrate application of passive seismic interferometry with the scattered diffuse wavefield, we used passive seismic data acquired in the XSoDEx experiment and applied the SNRS algorithm ~~of~~for EGFs evaluation. From the XSoDEx lines, one is particularly suitable for such demonstration. In this short high-resolution profile (green line in Fig. 9) of total length of 1000 m both 1C and 3C Sercel wireless units were installed at distances of 10 m. The 3C sensors were installed between 1C sensors at distances varying from 20 to 30 m. The results of passive seismic interferometry along this line can be also verified using the active source seismic data acquired along the same line and results of previous geophysical experiments and drilling in this area. The workflow for data analysis used in our paper is shown in Fig. 10.

For retrieving of EGFs and further ~~For~~ dispersion curve calculation, we used continuous passive seismic data recorded during the period of 21.08.2017 – 23.08.2017 (about 48 hours). We made no ~~any~~ *a-priori* assumptions about the nature and spatial distribution of noise sources. For calculation of EGFs, we applied such pre-processing procedures as removing mean and trend, spectral whitening and pre filtering by the band pass filter of 1-100 Hz. After this, we calculated crosscorrelation functions so that virtual sources of impulse signal were placed in the beginning, in the middle and in the end of the profile. The choice of virtual source positions is based on the wavelength of the analysed signal, which is about 400m. An example of EGFs calculated with the SNRS algorithm and the correspondent dispersion curve are presented in Figure 1011.

As seen from particle motion diagram calculated for one of the 3C sensors, the main arrival seen in EGFs corresponds to Rayleigh wave. A good ~~correlation-coherence~~ of waveforms of dispersed surface wave is also seen.

For calculation of velocity models from these three dispersion curves, we used Geopsy software (www.geopsy.org). We applied global optimization algorithm with 500 iterations to obtain the best solution. The starting model consisted of three major layers with properties presented in Table 1. The range of each property was selected using information about physical properties of rocks in the study area available from literature (Schön, 2015).

Table 1 – Starting model of the medium, used for inversion of dispersion curves.

Depth	Vp, m/s	Vs, m/s	Rho, kg/m ³	rock types
1-50	700-1200	350-900	1200-1500	quaternary deposits, coarse-grained sorted sediments
50-200	5900-6200	1800-3600	2000-2300	granite, felsic volcanic rocks

Formatted: English (United Kingdom)

Formatted: Font: Italic, English (United Kingdom)

Formatted: English (United Kingdom)

Formatted: English (United Kingdom)

Formatted: English (United Kingdom)

Formatted: English (United Kingdom)

Formatted: English (United Kingdom)

Formatted: English (United Kingdom)

Formatted: English (United Kingdom)

Formatted: English (United Kingdom)

Formatted: English (United Kingdom)

Formatted: English (United Kingdom)

Formatted: English (United Kingdom)

Formatted: English (United Kingdom)

Formatted: English (United Kingdom)

Formatted: English (United Kingdom)

Formatted: English (United Kingdom)

Formatted: English (United Kingdom)

200-500	6300-6600	3300-3600	2000-2500	mafic volcanic rocks
---------	-----------	-----------	-----------	----------------------

We calculated 1D velocity models for ~~receivers at~~ each 100 m of the profile, ~~using position of virtual sources at 0 m and 900 m (Figure 11 (a)). After that is, we and~~ obtained a 2D model presented on Figure 1412(a). The subplots 1412(b) and 1412(c) present results of global optimization of one selected dispersion curve. One interesting feature of this model is a layer with S-wave velocities of about 200-400 m/s and thickness of 20-38 m that may correspond to ~~thick~~ sediments. The thickness of sediments agrees well with the result of Åberg et al. (2017), who used GPR measurements and drilling information to obtain sedimentary thickness in this area. The velocities of S-waves beneath sedimentary cover will be discussed in Section 5.

We applied the same technique of EGFs calculation to the data with lower spatial resolution recorded along the part of Sakatti profile shown by blue in Figure 9. Particle motion diagram (Figure 14213(c)) shows that evaluated EGFs contain mainly surface waves. Dispersion curves were calculated for each 500 m of the profile for obtaining 2D velocity model. For this, the virtual sources were placed at each 500 m and all ~~neighbour~~ neighbor receivers, located at distances no ~~larger~~ longer than 1000 m from the virtual source receivers. For calculation of dispersion curves, ~~the~~ MASW technique was used.

As one can see in Figure 14213, ~~our advanced~~ method of passive seismic interferometry allowed ~~to us~~ to evaluate dispersion curve for frequencies of about 3-7 Hz. Inversion of dispersion curves was used to obtain 1D velocity models that were combined into ~~a~~ 2D model (Figure 14314(a)).

For verification of the modelling results we compared the velocity model in Figure 14314(a) with the model obtained by inversion of dispersion curves estimated from surface waves produced by ~~scattering of signal from~~ the controlled source for the same part of Sakatti line (Figure 14314 (b)). ~~We compared velocity models, because they are obtained at it is the last step of data processing, where all errors from previous steps are accumulated. In addition, we noticed that, At the same time, the differences between EGFs and dispersion curves for these two data sets are insignificant, there are not evidence differences.~~

As seen, the velocity models reveal the same details and the velocities are generally in good agreement. ~~From Figure 14213 (b) one can see that the width of error bars of dispersion curves are about 500 m/s. Differences in velocities between two 2D models (figure 14314) are within these limits.~~ The differences in velocities are of the order of 100 m/s in the central part of the profile. The largest difference up to 600 m/s can be seen in the beginning of the profile (from 15000 to 15500 m) and it can be explained either by uncertainty in dispersion curves extraction or by inversion errors.

6 Shear-wave velocity models obtained using Vibroseis ~~Q~~vibrotrack signal scattered at heterogeneities

Surface waves recorded in active source experiments (ground roll) usually considered as non-wanted signal and removed from the data during processing. However, S-wave velocity models can be obtained from Vibroseis© surface waves using MASW method (Al-Husseini et al., 1981; Mari, 1984; Gabriels et al., 1987; Park et al., 1999). In this case, the depth resolution for S-wave velocity models is limited to several meters due to short offsets and small registration time in near-vertical reflection data. As the data in XSoDEX experiment was recorded at long offsets with the wireless equipment, such recordings can be used to obtain the S-wave velocities at larger depths.

- Formatted: English (United Kingdom)
- Formatted: English (United Kingdom)
- Formatted: English (United Kingdom)
- Formatted: English (United Kingdom)
- Formatted: English (United Kingdom)
- Formatted: English (United Kingdom)

- Formatted: English (United Kingdom)
- Formatted: English (United Kingdom)
- Formatted: English (United Kingdom)
- Formatted: English (United Kingdom)
- Formatted: English (United Kingdom)

- Formatted: English (United Kingdom)
- Formatted: English (United Kingdom)

Examples of raw shot gathers of Vibroseis© signals recorded in reflection experiment are presented in Buske et al. (2019).
260 They used bandpass filters of 30-40-100-120 Hz to eliminate surface waves from raw reflection data. Vibrator sweep frequencies were from 10 to 170 Hz. In raw reflection data the surface waves arrivals can be followed up to 2-3 sec to rather short offsets of about 350 - 400 m. An example of record section compiled from wireless recorders data [deployed at 160 m interstation distances](#) is presented in Figure [14-15](#). In this section a vibrator signal, presented in Figure [45-16](#), was correlated with the traces recorded at long offsets. ~~The distance between traces in Figure 14-15 is 160 m.~~ In Figure [14-15](#) one can see the
265 first arrival of P-wave with velocity of about 5400 m/s and direct Rayleigh wave with velocity of about 880 m/s in frequency band of 20–100 Hz (Figure [14-15 \(b\)](#)) that can be followed to offsets of about 1 km. In the frequency band of 1-10 Hz (Figure [14-15 \(a\)](#)), surface waves cannot be followed to long offsets. The surface wave arrivals that can be correlated appear on several traces [at short offsets, close to shot](#). As seen in Figure [45-16 \(b\)](#), the frequencies of the vibrator signal start from about 12 Hz and no lower frequencies are present.

270 We used the SNRS technique and continuous seismic recordings of XSoDEx experiment to obtain EGFs for all the XSoDEx profiles. In all EGFs the main phase seen was Rayleigh wave (Figure [46-17](#)). The EGFs were used to obtain dispersion curves and invert them using Geopsy inversion software and model parameters, presented in Table 1. The 2D velocity models to the depth of 300 m for all XSoDEx profiles obtained by interpolation of 1D velocity models are presented in Figure [47-18](#), in which also the boundaries of major lithological units from Figure 1 are indicated. All the velocity models are shown in the same
275 colour scale. The S-wave velocities along the XSoDEx are generally varying from very low values of 200-400 m/s detected in some places to 3200 m/s. The uppermost layer with velocities of 200-400 m/s and thickness up to 50 m corresponds to quaternary sediments, and the boundary between this layer and the lowermost part of velocity models is indicated also by velocity contrast in 1D models. Independent information about thickness of sediments in our study area obtained by direct drilling shows that the thickness of quaternary sediments there is ~~limited to several no more than 40-50 dozens dozen~~ meters.

280 That is why it can be concluded that S-wave velocities in the range of 800-3200 m/s correspond to different types of basement rocks. As these values are generally much lower than the values of S-wave velocities for the rocks of Fennoscandian Shield obtained by laboratory measurements on rock samples (Kern et al., 1993, Dortman, 1992), they cannot be interpreted directly in terms of rock composition.

One possible explanation is that the low values of shear wave velocities might be caused by non-zero azimuths to noise sources.
285 However, it was demonstrated by previous studies that non-zero azimuth increases apparent velocity (e.g. Sadeghisorkhani et al., 2016). That is why it is necessary to find another explanation of generally low S-wave velocities of the basement rock in our study.

[The S-wave velocities in the uppermost crust down to several kilometers were previously evaluated using surface waves by Pedersen and Campillo \(1991\), Grad and Luosto \(1992\), Grad et al. \(1998\).](#) They reveal low values of S-wave velocity in the
290 shallow crust and low values of quality factor that is rapidly increasing at the depth of about 1 km. Moreover, Grad et al. (1998) found that the quality factor in the Archean shallow crust of the Fennoscandian Schield is lower than that in the Proterozoic crust. Grad and Luosto (1992) explained the low quality factor in the uppermost 1 km of the crust by increased cracks density.

Formatted: English (United Kingdom)

Formatted: English (United Kingdom)

Formatted: English (United Kingdom)

Therefore, increased crack density can explain also generally low S-wave velocities of the basement rocks revealed by our study. Consider that the wave is propagating through fractured medium consisting of granites and the fractures are filled with some clastic rocks. If the S-wave velocities in the granitic rock are about 3300 m/s and those in the clastic rocks are about 400 m/s (similar to the velocity in quaternary deposits), then the averaged velocity would be about 1700-2000 m/s, depending on crack density. Taking the general effect of fracturing into account, we conclude that the values of S-wave velocities lower than 2000 m/s correspond to felsic rock, while the higher values of velocity correspond to mafic and ultramafic rocks (Figure 1718).

7 Conclusions

In our study, we used recordings of ambient noise recorded during short time period in a generally quiet area with low level of anthropogenic noise. We showed that the noise was non-stationary and the azimuthal distribution of noise sources was neither isotropic nor heterogeneous during the whole data acquisition period. In spite of that, we obtained good quality EGFs and dispersion curves and the S-wave velocity models showing presence and thickness of quaternary sedimentary cover and velocity heterogeneities in the bedrock that agree well with the geological data. We explain this by the fact that the ambient noise recorded during the XSoDEx experiment contained a large proportion of diffused wavefield produced by scattering of plane waves from distant sources and ballistic waves produced by certain types of non-stationary sources on stochastically distributed heterogeneities in the uppermost crust. We demonstrated by numerical modelling that certain types of geological structures, particularly those composed of rocks with contrasting elastic properties, could scatter plane waves and ballistic waves from non-stationary sources and produce scattered Rayleigh waves. This scattered wavefield together with the ballistic wavefield from non-stationary sources can be used for EGFs evaluation, if the special algorithm of signal-to-noise ratio stacking (SNRS) is applied. Our result is a practical illustration of the conclusions about retrieval of EGF from the scattered wavefield revealed previously by Wapenaar (2004) and Wapenaar and Thorbecke (2013). In certain geological areas, extraction of EGFs from the wavefield scattered at heterogeneities provides an opportunity to reduce the time for short-term passive seismic experiments.

8 Acknowledgements

The XSoDEx project was realised as a joint effort of Geological Survey of Finland (coordinator), TU Bergakademie Freiberg, Institute of Geophysics and Geoinformatics, Freiberg, Germany, and University of Oulu. The wireless equipment of the University of Oulu is jointly operated by Oulu Mining School and Sodankylä Geophysical Observatory of the University of Oulu. The field work of the University of Oulu personnel in summer, 2017 was supported by the Renlund Foundation. Financial support for processing and interpretation of the XSoDEx data used in this study was provided by Geological Survey of Finland in 2018. Thanks to Sodankylä Geophysical Observatory staff for their kind assistance during XSoDEx survey. Particular thanks are to Hanna Silvennoinen, Jouni Nevalainen, Kari Moisio, Jari Karjalainen and Tommi Pirttisalo, whose participation in

XSoDEx field survey was particularly important for safe and reliable operation of Sercel Ltd wireless equipment. Many thanks
325 to Henrik Jänkäväära for his contribution in XSoDEx data processing.
The authors wish to acknowledge CSC – IT Center for Science, Finland, for computational resources. The numerical modelling
of wavefields, presented in the work was funded by the Russian Ministry of Education and Science by a research project of
state assignment ‘Development of seismic methods for forecasting and reducing the consequences of natural and man-made
disasters in the Western Arctic sector of the Russia’ (0409-2015-0135, №AAAA-A18-118012490072-7).

330 **References**

Åberg, A. K., Salonen, V. P., Korkka-Niemi, K., Rautio, A., Koivisto, E., Åberg, S. C.: GIS-based 3D sedimentary model for
visualizing complex glacial deposition in Kersilö, Finnish Lapland, Boreal environment research, 22, 277-298,
http://hdl.handle.net/10138/257516, 2017

Abraham, E. M., Alile, O. M.: Modelling subsurface geologic structures at the Ikogosi geothermal field, southwestern Nigeria,
335 using gravity, magnetics and seismic interferometry techniques, Journal of Geophysics and Engineering, 16(4), 729-741,
https://doi.org/10.1093/jge/gxz034, 2019

Afonin, N., Kozlovskaya, E., Kukkonen, I., and DAFNE/FINLAND Working Group: Structure of the Suasselkä postglacial
fault in northern Finland obtained by analysis of local events and ambient seismic noise, Solid Earth, 8, 531–544,
https://doi.org/10.5194/se-8-531-2017, 2017.

340 Afonin, N., Kozlovskaya, E., Nevalainen, J., Narkilahti, J.: Improving the quality of empirical Green's functions, obtained by
cross-correlation of high-frequency ambient seismic noise, Solid Earth, 10(5), 1621-1634, https://doi.org/10.5194/se-10-1621-
2019, 2019.

Aki, K.: Analysis of the seismic coda of local earthquakes as scattered waves. Journal of geophysical research, 74(2), 615-
631, 1969

345 Aki, K., Richards, P. G.: Quantitative seismology, 2002.

Al-Husseini, M. I., Glover, J. B., Barley, B. J.: Dispersion patterns of the ground roll in eastern Saudi Arabia, Geophysics,
46.2, 121-137, https://doi.org/10.1190/1.1441183, 1981

Antonovskaya, G.N., Kapustian, N.K., Moshkunov, A.I., Danilov, A.V., Moshkunov, K.A.: New seismic array solution for
earthquake observations and hydropower plant health monitoring, Journal of Seismology, 21, 1039–1053,
350 https://doi.org/10.1007/s10950-017-9650-8, 2017

Antonovskaya, G., Kapustian, N., Basakina, I., Afonin, N., Moshkunov, K.: Hydropower Dam State and Its Foundation Soil
Survey Using Industrial Seismic Oscillations, Geosciences, 9(4), 187, https://doi.org/10.3390/geosciences9040187, 2019

Buske, S., Hlousek, F., Jusri, T., XSoDEx: Reflection seismic data acquisition and processing report, Institute of Geophysics
and Geoinformatics TU Bergakademie Freiberg, Germany, 57 pp., 2019

Formatted: English (United Kingdom)

Formatted: English (United Kingdom)

Formatted: English (United Kingdom)

355 [Bohlen, T., Mueller, Ch. And Milkereit, B.: Elastic Seismic Wave Scattering from Massive Sulfide Orebodies. On the role of Composition and Shape. In: Eaton, D.W., Milkereit, B., and Salisbury, M. Hardrock Seismic Exploration. Geophysical Developments No. 10, Society of Exploration Geophysics, pp. 70-89, 2003.](#)

Campillo, M., and Paul, A.: Long-range correlations in the diffuse seismic coda, *Science*, 299(5606), 547-549, DOI: 10.1126/science.1078551, 2003

360 Cheraghi, S., White, D. J., Draganov, D., Bellefleur, G., Craven, J. A., Roberts, B.: Passive seismic reflection interferometry: A case study from the Aquistore CO2 storage site, Saskatchewan, Canada, *Geophysics*, 82(3), B79-B93, <https://doi.org/10.1190/geo2016-0370.1>, 2017

Dantas, O. A. B., do Nascimento, A. F., Schimmel, M.: Retrieval of body-wave reflections using ambient noise interferometry using a small-scale experiment, *Pure and Applied Geophysics*, 175(6), 2009-2022, [https://doi.org/10.1007/s00024-018-1794-](https://doi.org/10.1007/s00024-018-1794-0)

365 0, 2018

Dortman, N. B.: *Handbook Petrophysics*, Nedra, Moscow, 390 pp, 1992

Draganov, D., Campman, X., Thorbecke, J., Verdel, A., Wapenaar, K.: Reflection images from ambient seismic noise, *Geophysics*, 74(5), 63–67, <https://doi.org/10.1190/1.3193529>, 2009

[Frankel, A., Clayton, R. W.: Finite difference simulations of seismic scattering: Implications for the propagation of short-](#)

370 [period seismic waves in the crust and models of crustal heterogeneity. *Journal of Geophysical Research: Solid Earth*, 91\(B6\), 6465-6489, 1986](#)

Gabriels, P., Snieder, R., Nolet, G.: In situ measurements of shear-wave velocity in sediments with higher-mode Rayleigh waves, *Geophysical prospecting*, 35.2, <https://doi.org/10.1111/j.1365-2478.1987.tb00812.x>, 187-196, 1987

Grad, M., and Luosto, U.: Fracturing of the crystalline uppermost crust beneath the SVEKA profile in Central Finland, *Geophysica*, 28.1-2, 53, 1992

375 Grad, M., Czuba, W., Luosto, U., Zuchniak, M.: QR factors in the crystalline uppermost crust in Finland from Rayleigh surface waves, *Geophysica*, 34(3), 115-129, 1998

[Grêt, A., Snieder, R., Aster, R. C., Kyle, P. R.: Monitoring rapid temporal change in a volcano with coda wave interferometry, *Geophysical Research Letters*, 32\(6\), <https://doi.org/10.1029/2004GL021143>, 2005](#)

380 Grêt, A., Snieder, R., Scales, J.: Time-lapse monitoring of rock properties with coda wave interferometry, *Journal of Geophysical Research: Solid Earth*, 111(B3), <https://doi.org/10.1029/2004JB003354>, 2006

Kern, H., Walther, C., Flüh, E. R., Marker, M.: Seismic properties of rocks exposed in the POLAR profile region—constraints on the interpretation of the refraction data, *Precambrian Research*, 64 (1-4), 169-187, [https://doi.org/10.1016/0301-9268\(93\)90074-C](https://doi.org/10.1016/0301-9268(93)90074-C), 1993

385 Leväniemi, H., Melamies, M., Mertanen, S., Heinonen, S., Karinen, T.: Petrophysical measurements to support interpretation of geophysical data in Sodankylä, northern Finland, *Geological Survey of Finland Open File Work Report 25/2018*, 2018

[Lobkis, O. I., Weaver, R. L.: On the emergence of the Green's function in the correlations of a diffuse field. *The Journal of the Acoustical Society of America*, 110\(6\), 3011-3017, 2001](#)

Formatted: English (United Kingdom)

390 Mari, J. L.: Estimation of static corrections for shear-wave profiling using the dispersion properties of Love waves, *Geophysics*,
49(8), 1169-1179, <https://doi.org/10.1190/1.1441746>, 1984

Oren, C. and Nowack, R. L., Seismic body-wave interferometry using noise auto-correlations for crustal structure, *Geophysical Journal International*, 208(1), 321-332, <https://doi.org/10.1093/gji/ggw394>, 2016

395 Park, C. B., Miller, R. D., Xia, J.: Multichannel analysis of surface waves, *Geophysics*, 64(3), 800-808,
<https://doi.org/10.1190/1.1444590>, 1999

Payan, C., Garnier, V., Moysan, J., Johnson, P. A.: Determination of third order elastic constants in a complex solid applying coda wave interferometry, *Applied Physics Letters*, 94(1), 011904, <https://doi.org/10.1063/1.3064129>, 2009

Pedersen, H., and Campillo, M.: Depth dependence of Q beneath the Baltic Shield inferred from modeling of short period seismograms, *Geophysical research letters*, 18.9, 1755-1758, <https://doi.org/10.1029/91GL01693>, 1991

400 Planès, T., Obermann, A., Antunes, V., Lupi, M.: Ambient-noise tomography of the Greater Geneva Basin in a geothermal exploration context, *Geophysical Journal International*, 220(1), 370-383, <https://doi.org/10.1093/gji/ggz457>, 2020

Poli, P., Pedersen, H. A., Campillo, M., POLENET/LAPNET Working Group.: Emergence of body waves from cross-correlation of short-period seismic noise, *Geophysical Journal International*, 188(2), 549-558, <https://doi.org/10.1111/j.1365-246X.2011.05271.x>, 2012

405 Polychronopoulou, K., Lois, A., Draganov, D.: Body-wave passive seismic interferometry revisited: mining exploration using the body waves of local microearthquakes, *Geophysical Prospecting* 68.1-Cost-Effective and Innovative Mineral Exploration Solutions, 232-253, <https://doi.org/10.1111/1365-2478.12884>, 2020

Reid, K. J.: *The Importance of Minerals and Mining*, Online Lecture, University of Minnesota, 2011

Rickett, J. and Claerbout, J.: Acoustic daylight imaging via spectral factorization: helioseismology and reservoir monitoring, *Geophysics*, 18, 957-960, <http://dx.doi.org/10.1190/1.1438420>, 1999

410 Romero, P. and Schimmel, M.: Mapping the basement of the Ebro Basin in Spain with seismic ambient noise autocorrelations, *Journal of Geophysical Research: Solid Earth*, 123(6), 5052-5067, <https://doi.org/10.1029/2018JB015498>, 2018

Roots, E., Calvert, A. J., Craven, J.: Interferometric seismic imaging around the active Lalor mine in the Flin Flon greenstone belt, Canada, *Tectonophysics*, 718, 92-104, <https://doi.org/10.1016/j.tecto.2017.04.024>, 2017

415 Roux, P., Sabra, K.G., Gerstoft, P., Kuperman, W.A., Fehler, M.C.: P-waves from cross-correlation of seismic noise, *Geophysical Research Letters*, 32, L19303, doi:10.1029/2005GL023803, 2005

Ruigrok, E., Campman, X., Wapenaar, K.: Extraction of P-wave reflections from microseisms, *Comptes Rendus Geoscience*, 348(8-9), 512-525, <https://doi.org/10.1016/j.crte.2011.02.006>, 2011

Sadeghisorkhani, H., Gudmundsson, Ó., Roberts, R., Tryggvason, A.: Mapping the source distribution of microseisms using noise covariogram envelopes, *Geophysical Journal International*, 205(3), 1473-1491, <https://doi.org/10.1093/gji/ggw092>, 2016

420 Shapiro, N. and Campillo, M.: Emergence of broadband Rayleigh waves from correlations of the ambient seismic noise, *Geophysical Research Letters*, 31.7, <https://doi.org/10.1029/2004GL019491>, 2004

Formatted: English (United Kingdom)

Formatted: English (United Kingdom)

Formatted: English (United Kingdom)

Schön, J.H.: Fundamentals and principles of petrophysics, 2nd edition. Elsevier, 512 pp, 2015

Snieder, R., Grêt, A., Douma, H., Scales, J.: Coda wave interferometry for estimating nonlinear behavior in seismic velocity,

Science, 295(5563), 2253-2255, DOI: 10.1126/science.1070015, 2002

Snieder, R.: The theory of coda wave interferometry, Pure and Applied geophysics, 163(2-3), 455-473, <https://doi.org/10.1007/s00024-005-0026-6>, 2006

Taylor, G., Rost, S., Houseman, G.: Crustal imaging across the North Anatolian Fault Zone from the autocorrelation of ambient seismic noise, Geophysical Research Letters, 43, 2502–2509, <https://doi.org/10.1002/2016GL067715>, 2016

Tibuleac, I. M. and von Seggern, D.: Crust–mantle boundary reflectors in Nevada from ambient seismic noise autocorrelations, Geophysical Journal International, 189(1), 493–500, <https://doi.org/10.1111/j.1365-246X.2011.05336.x>, 2012

van Manen, D. J., Curtis, A., Robertsson, J. O.: Interferometric modeling of wave propagation in inhomogeneous elastic media using time reversal and reciprocity, Geophysics, 71(4), SI47-SI60, <https://doi.org/10.1190/1.2213218>, 2006

Vasara, H.: State and outlook of the mining industry, MEAE Business Sector Services, Spring 2018, Sector Reports, Ministry of Economic Affairs and Employment of Finland, <http://urn.fi/URN:ISBN:978-952-327-297-2>, 2018

Wang, T., Song, X., Han, H. X.: Equatorial anisotropy in the inner part of Earth’s inner core from autocorrelation of earthquake coda, Nature Geoscience, 8, 224-227, <https://doi.org/10.1038/ngeo2354>, 2015

Wapenaar, K.: Retrieving the Elastodynamic Green’s Function of an Arbitrary Inhomogeneous Medium by Cross Correlation, Physical review letters, 93(25), 254301, <https://link.aps.org/doi/10.1103/PhysRevLett.93.254301>, 2004

Wapenaar, K., Van Der Neut, J., Ruigrok, E., Draganov, D., Hunziker, J., Slob, E., Snieder, R.: Seismic interferometry by crosscorrelation and by multidimensional deconvolution: A systematic comparison, Geophysical Journal International, 185(3), 1335-1364, <https://doi.org/10.1111/j.1365-246X.2011.05007.x>, 2011

Wapenaar, K. and Thorbecke, J.: On the retrieval of the directional scattering matrix from directional noise, SIAM Journal on Imaging Sciences, 6(1), 322-340, <https://doi.org/10.1137/12086131X>, 2013

[Wu, R. S., Aki, K.: Scattering characteristics of elastic waves by an elastic heterogeneity. Geophysics, 50\(4\), 582-595, 1985](#)

Formatted: English (United Kingdom)

Formatted: English (United Kingdom)

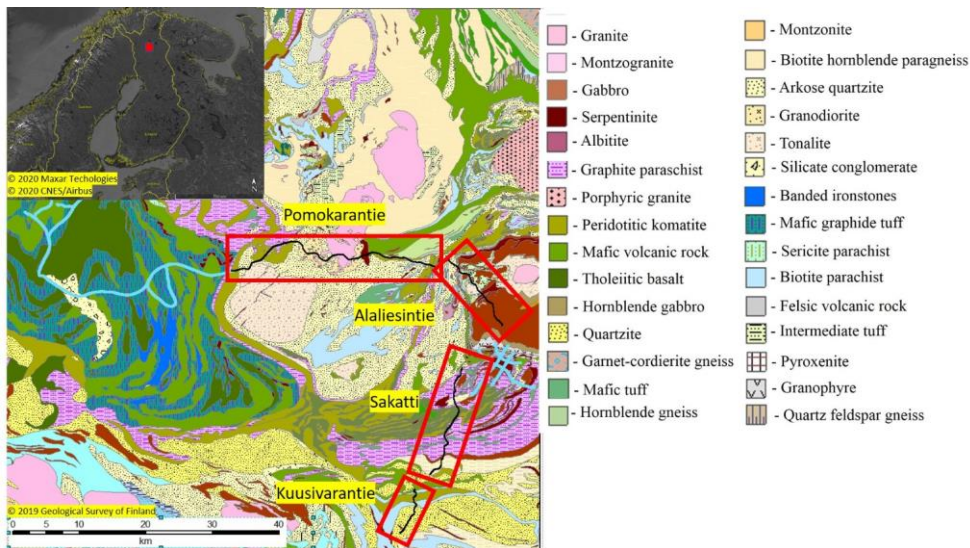


Figure 1: Geological map of XSoDEX study area (Buske et. al., 2019). The XSoDEX survey lines are shown with black lines. Previous seismic reflection survey lines are plotted with blue lines.

Field Code Changed

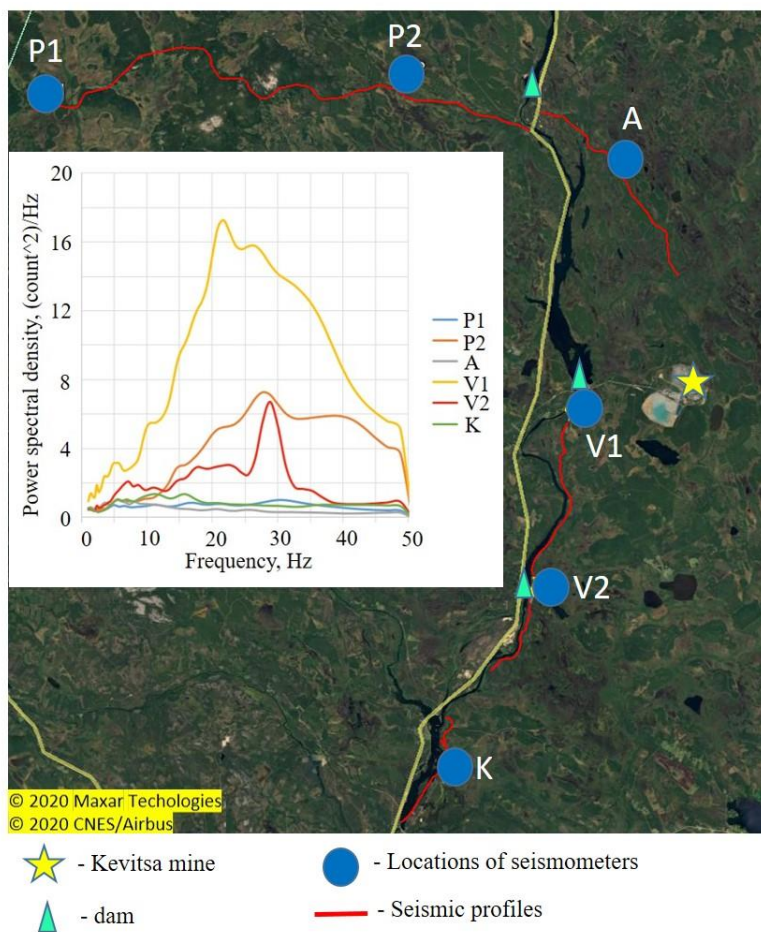


Figure 2: Illustration of noise level at four stations located in different profiles of XSoDEx experiment. Position of strong noise sources (Kevitsa mine and dams of water power stations) and seismic stations selected for analysis are indicated. Yellow lines show roads. Inset figure shows comparison of ambient noise power spectral density estimated at selected stations.

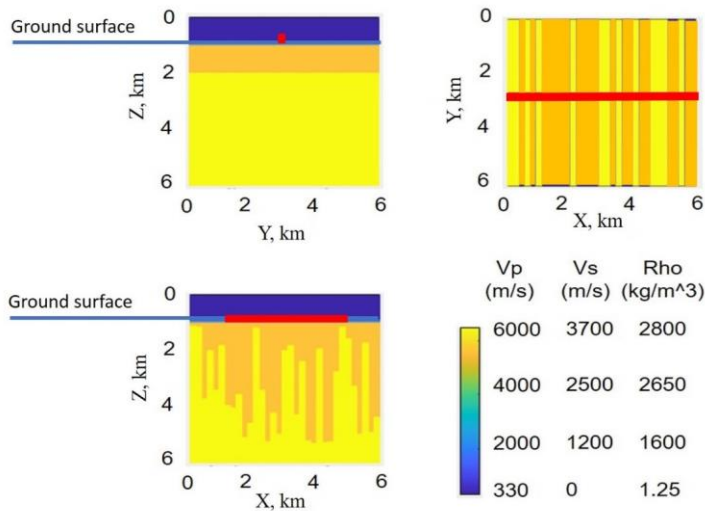


Figure 3: The synthetic model used for investigation of wave propagation. Position of the seismic profile marked by the red line. Low velocity corresponding to the air is indicated on the top by blue colour.

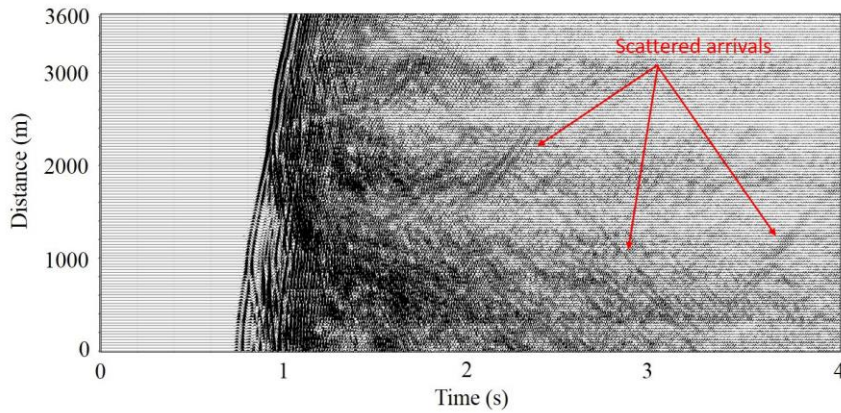


Figure 4: An example of synthetic seismogram (vertical component) of plane wave arrived with incidence angle of approach of 45 degree and propagated through the synthetic model (0-4 sec). The seismogram shows, first arrivals and numerous reflections. From about 1.5 seconds we can see scattered arrivals of different directions with apparent velocities of 2100 -2500 m/s. Several arrivals of scattered waves are indicated marked by red arrows yellow lines.

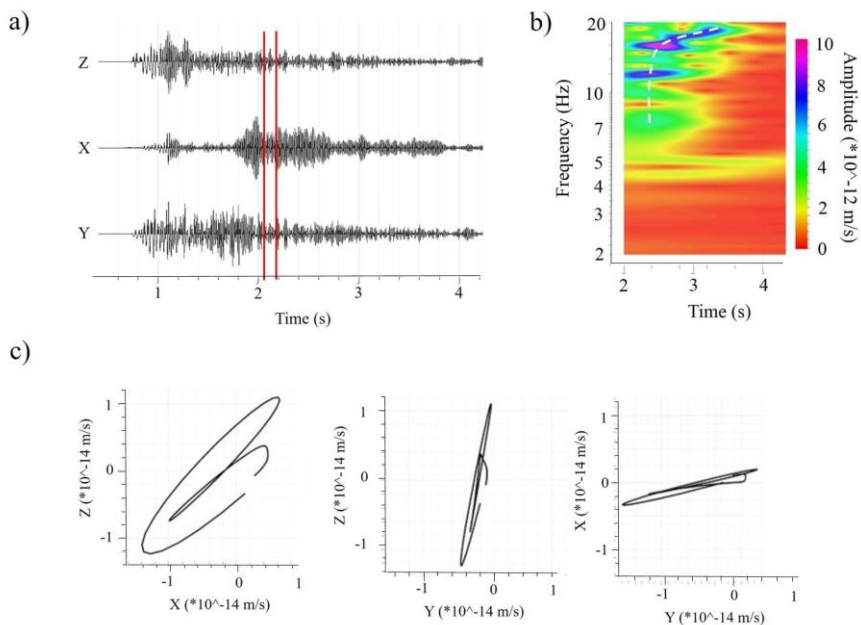


Figure 5: Result of analysis of scattered arrivals in synthetic seismograms with apparent velocity of 2100 -2500 m/s for frequencies 2-20 Hz in (Fig. 4): a) 3C seismogram for synthetic receiver located, recorded at distance of 2000 m from the source in the seismogram shown in (Figure 4); b) spectrogram of the scattered arrival, recorded by vertical component of synthetic receiver (white dashed line illustrate dispersion properties of the scattered arrival corresponds to dispersion curve, picked by amplitude maximums); c) particle motion diagrams, calculated using part of seismogram indicated by red lines in Figure 5 (a), which corresponds to scattered wavefield arrival.

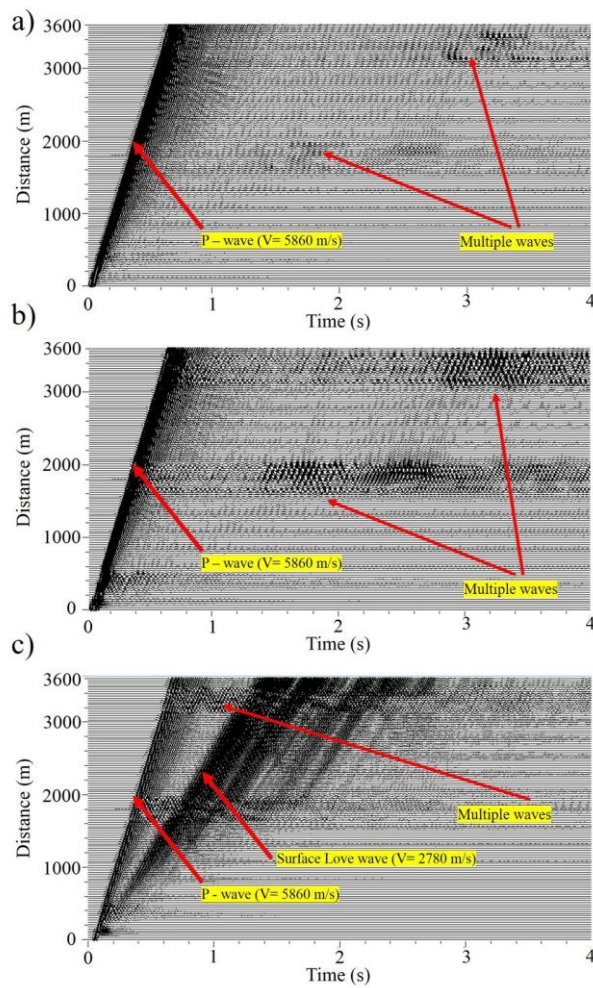


Figure 6: Synthetic seismograms of the blast: a) vertical channel Z; b) horizontal channel X; c) horizontal channel Y.

Formatted: English (United Kingdom)

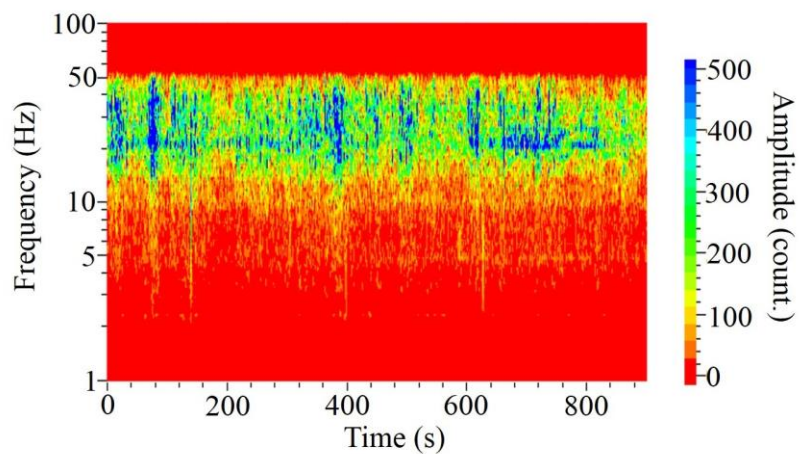


Figure 7: Spectrogram of the signal recorded by station V1 ([location is shown in Figure 2](#)) and used as a wavefield of the source in simulation.

Formatted: English (United Kingdom)

Formatted: English (United Kingdom)

Formatted: English (United Kingdom)

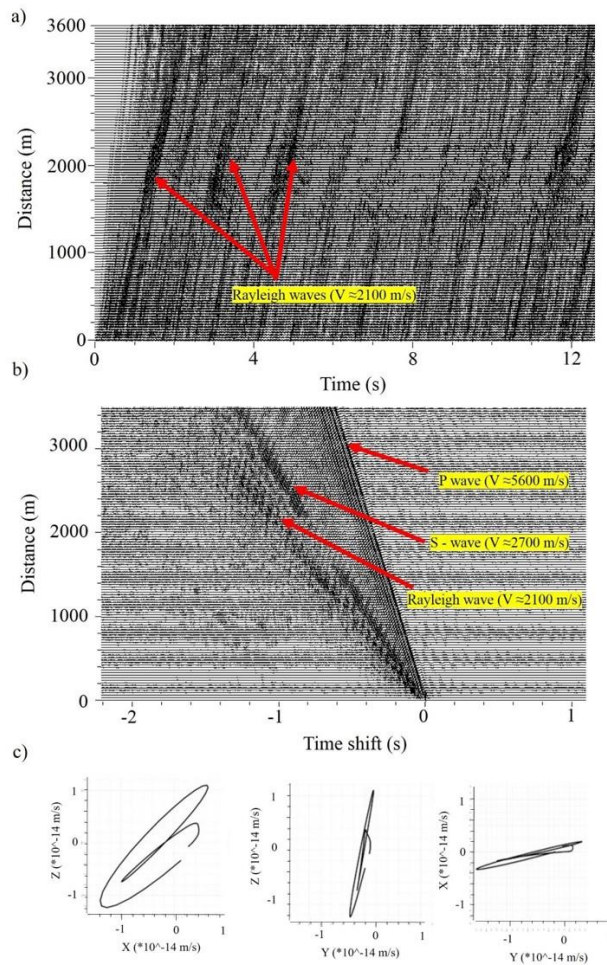


Figure 8: Synthetic seismograms of the signal with the spectrogram presented in Fig. 7 and propagating in synthetic model shown in Fig. 3: a) seismograms of vertical components; b) crosscorrelation functions of vertical components, calculated between the first and all other traces; c) particle motion diagram of Rayleigh wave.



Figure 9: Location of passive seismic profiles of XSoDEX Sakatti line: green line indicates high-resolution profile; blue line indicates profile of lower-resolution.

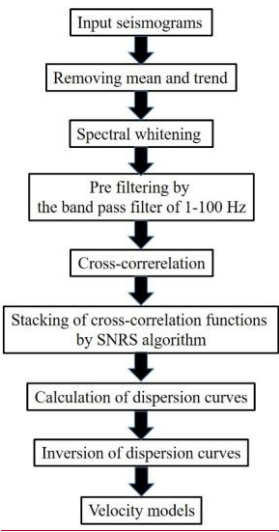


Figure 10: The workflow for data analysis

Formatted: English (United Kingdom)

Formatted: English (United Kingdom)

Formatted: English (United Kingdom)

Formatted: Normal

Formatted: Normal, Centered

Formatted: English (United Kingdom)

Formatted: Font: 9 pt, Bold, English (United Kingdom)

Formatted: Normal

Formatted: English (United Kingdom)

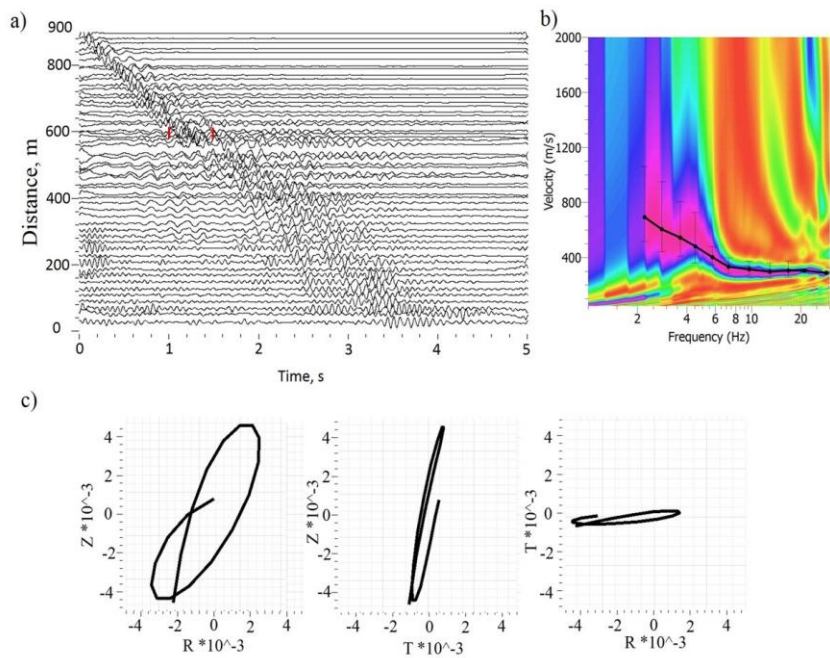
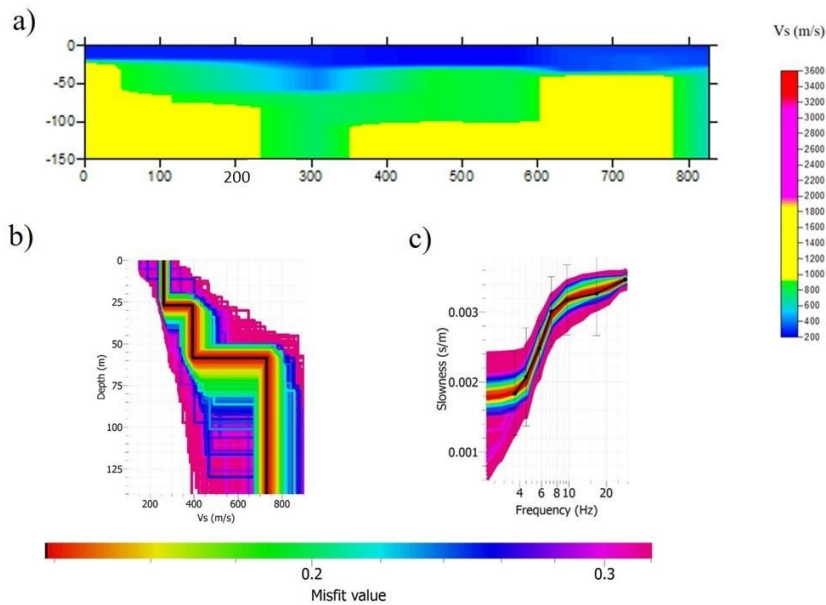


Figure 10.11: Example of EGFs with the correspondent dispersion curve, obtained from passive seismic data for high-resolution profile shown in Fig. 9: a) EGFs; b) dispersion curve, extracted by MASW technique; c) particle motion diagrams for part of EGF indicated in (a) by red lines.

Formatted: English (United Kingdom)

Formatted: English (United Kingdom)



490 **Figure H12:** Results of inversion of dispersion curves obtained from passive seismic data of high-resolution XSoDEx profile: a) 2D velocity model obtained by interpolation of 1D velocity models. Velocity colour scale is shown in the left. b) an example of 1D velocity model (black line) obtained by inversion of the dispersion curve in (c), corresponding to distance of 200 m in Fig. H12 (a); c) dispersion curve (black line), used for inversion of the velocity model in Fig. H12 (b). Colour scale corresponds to values of misfit function during different iteration steps in global optimization algorithm.

Formatted: English (United Kingdom)

Formatted: English (United Kingdom)

Formatted: English (United Kingdom)

Formatted: English (United Kingdom)

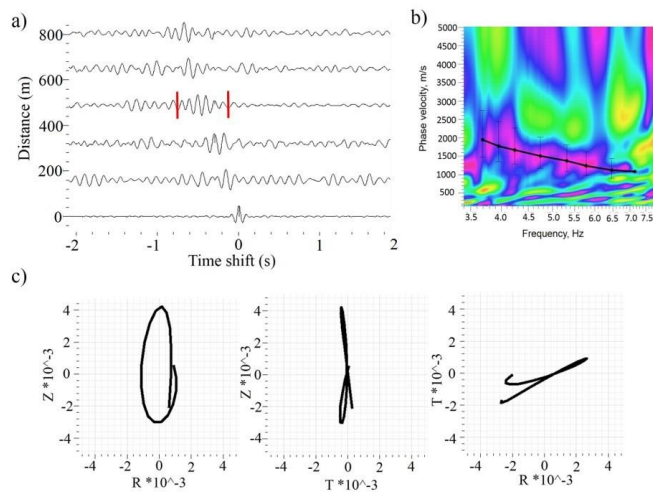


Figure 1213: Example of EGFs with correspondent dispersion curve, obtained from passive seismic data: a) EGFs on frequency band 3-8 Hz; b) dispersion curve, calculated from EGFs by MASW technique; c) particle motion diagrams of a surface wave part of an EGF indicated by red lines.

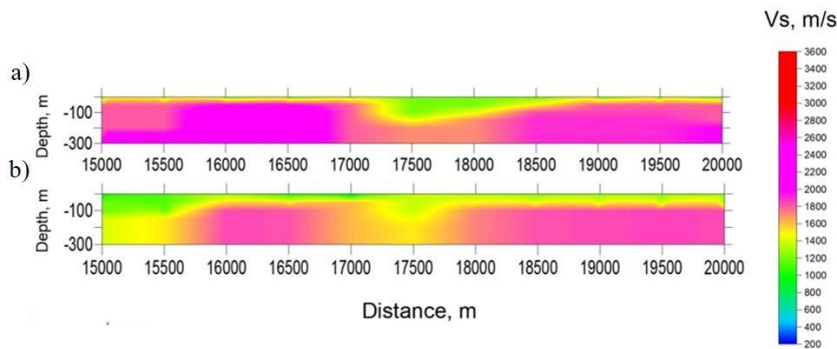


Figure 1314: Velocity models calculated by inversion of dispersion curves along the part of Sakatti profile marked by blue in Fig. 9. (a) S-wave velocity model obtained using passive seismic data; (b) S-wave velocity model obtained using controlled-source seismic data, which contain signals produced by controlled source.

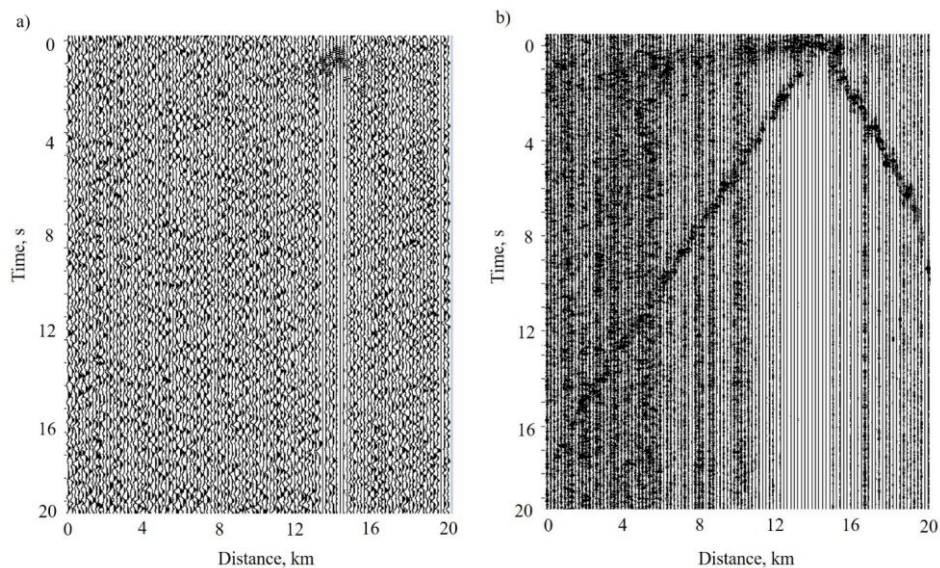


Figure 14.15: Crosscorrelation functions of signals, produced by Vibroseis© with the data recorded by wireless equipment at large offsets in frequency band of: a) 1-10 Hz, amplitudes normalized at maximum of each trace; b) 20-100 Hz. The signal used for cross correlation is shown in Fig. 14.16.

Formatted: English (United Kingdom)

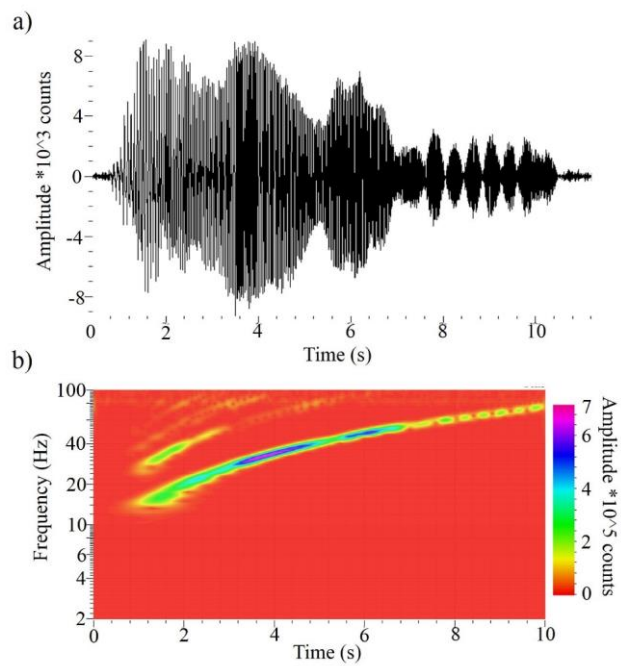


Figure 1516: An example of Vibroseis© sweep, recorded by a wireless sensor placed near the vibrator in XSoDEx experiment: a) seismogram; b) spectrogram showing the frequency content of a vibrator signal.

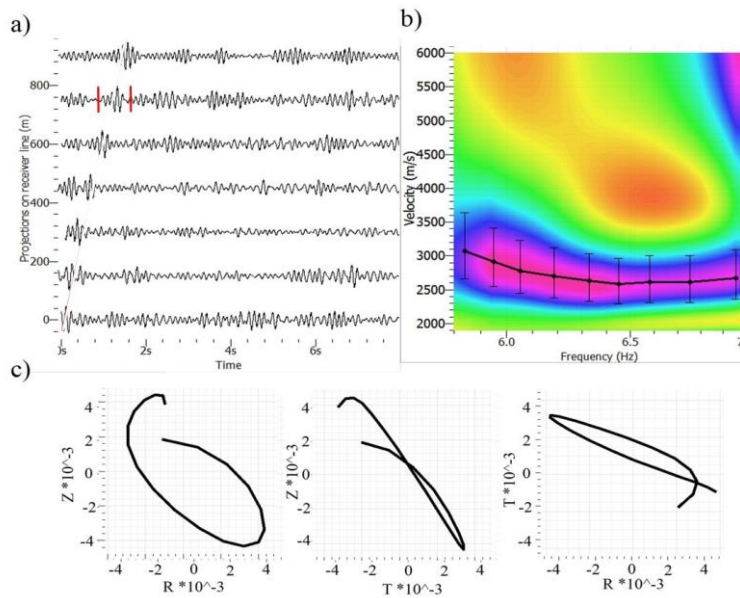
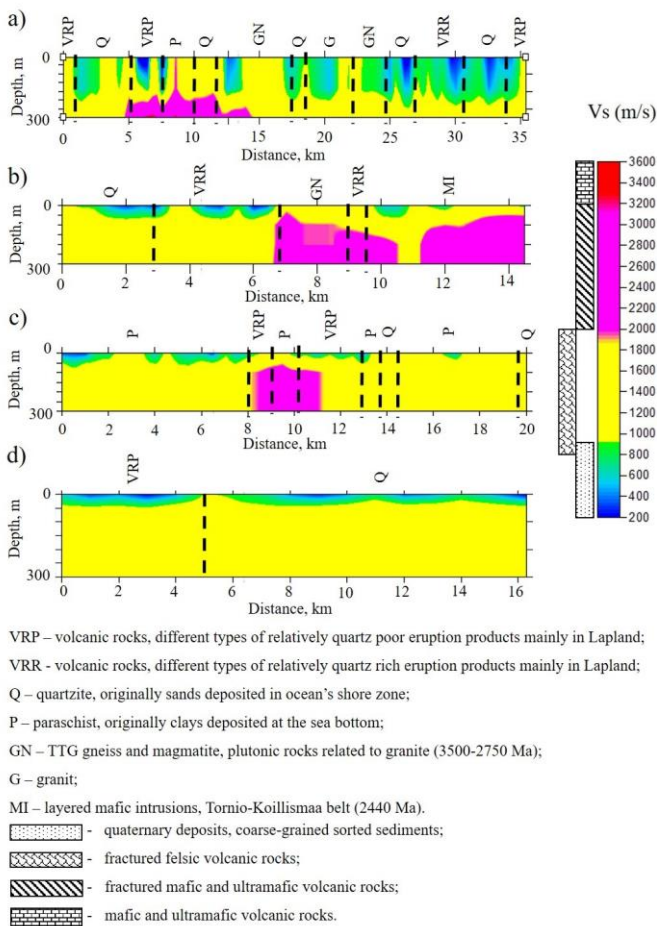


Figure 1617: An example of EGFs with correspondent dispersion curve of Rayleigh wave on frequency band 5-10 Hz, obtained by advanced method of passive seismic interferometry: a) EGFs; b) dispersion curve, extracted by MASW technique; c) particle motion diagrams for surface wave part of EGF marked by red in (a).



515 **Figure 4718:** Velocity models, calculated by inversion of dispersion curves, obtained by passive seismic interferometry for XSoDex profiles shown in Fig. 1. The boundaries of geological units are marked by black dashed lines: a) Pomokairantie; b) Alaliesintie; c) Sakatti; d) Kuusivaarantie.

520 **Author response to the interactive comment posted by Yunhuo Zhang (Referee)**

Referee: I have gone through the entire pre-print. It is an interesting study and useful reference. It can be considered for publication, provided some areas can be improved. Please refer below for your consideration: The title of the paper highlights the ‘advanced method’, which is the SNRS algorithm to estimate the green’s function from diffusive ambient noise field. However, the SNRS is just referred to the author’s earlier paper, without any elaboration. This makes the title not reflects the content correspondingly. Since the SNRS algorithm is already published and discussed earlier, it is suggested to amend the title accordingly, either highlighting the case study, or the attempts to characterize the noise field of the sites, etc.

530 **Authors:** The title of the manuscript has been changed by removing words “advanced method”. The new title is “Near surface structure of Sodankylä area in Finland, obtained by passive seismic interferometry”.

535 **Referee:** Section 4, several synthetic models are created to characterize the noise field of the site, taking into consideration of the nearby major activities. It is quite interesting and worth expanding. The assumptions of major sources need more explanation.

540 **Authors:** The assumption about major sources was made based on analysis of spectra, presented in the Section 3, and knowledge about locations of industrial objects, roads and other human activities. Moreover, we consider the universal source – plane wave, which is an approximation of any source located in the far field area. The corresponding text has been corrected.

545 **Referee:** The key message of creating the synthetic models are to support the claim that the noise field of site is diffusive. However, it is very common in elsewhere, too. Therefore, it would be better to draw some more novel conclusions from the synthetic models.

550 **Authors:** The main goal, except of supporting the claim that analyzed wavefield is diffuse, was also to understand how relatively high-frequency wave (dozens of Hz) may produce low-frequency (about 5-20 Hz) wavefield during scattering on heterogeneities. In our opinion, the previous synthetic modelling efforts published in literature were mainly focusing on scattering of waves from controlled sources (see, for example, Gritto et. al., 1995, Bohlen et al., 2003). In our modelling we were interested to see scattered wavefield from various types of sources, including plane wave from sources located in far field zone. In our modelling we also followed propagation of wave from these sources during time intervals that are longer than those typical for data acquisition in controlled source experiments. Spectral analysis of scattering arrivals (figure 5) shows that the plane wave with frequency of 40 Hz produces surface waves with frequencies of about 7-20 Hz during scattering. The corresponding text has been corrected.

560 **Referee:** Noted that each synthetic model is to simulate one type of sources. Would it better to create an overall model that combines all possible noise sources. If this one can be done, the authors may explore full waveform inversion of passive seismic waves.

Authors: It was shown in numerous studies (for example Wapenaar et al., 2004; Mulargia, 2012, etc.), that diffused wavefield is usually produced by the superposition of waves of numerous sources and scatterings on heterogeneities. We included these studies to the list of references. Nevertheless, our goal was to study the nature of low frequency wavefield, when all possible sources have relatively high frequencies.

Referee: It is essential to beef up the field acquisition in more and clearer details, e.g., the field plan out, geophone type and corner frequency, sampling rate, source signature and location for active testing, etc.

Authors: The chapter 2 (experiment description) has been revised and more details concerning experiment were added.

Referee: Figure 1 is not clear where are the blue/black lines. It is also difficult for the readers who are not familiar with Finland geology without necessary introduction.

Authors: The figure 1 has been changed

Referee: The quality of Figure 2 needs to be improved to meet the criteria of publication.

Authors: The figure 2 has been modified.

Referee: It is not clear about the caption of Figure 5 (a) that what is the distance of 2000m referring to. Figure 5(b) horizontal axis and color bar scale seem not correct, if it is a dispersion image.

Authors: Figure caption has been changed

Referee: Figure 6 (b) and 6 (c) are very interesting. It is worth expanding the explanation why these 2 directions are so different, whereby 6(b) can't see surface wave and 6 (c) can see surface wave clearly.

Authors: The synthetic model shows that the wave propagating from the considered source (blasts) inside the model that contains numerous irregular heterogeneities, produced only Love surface waves. In this modelling, the main objective was to clarify the absence of Rayleigh waves on seismograms, produced by blasts. The explanation of this phenomenon is not simple and might be the topic for another research and more enhanced modelling.

Referee: Figure 7 shows the source is mainly in 10-40 Hz, which is quite high. Please explain how such high frequency source can illuminate to 300 m below ground.

Authors: We show by synthetic modelling, how high-frequency waves are converted to low-frequency wavefield when scattering on heterogeneities (for example, we show that the plane wave with frequency

of 50 Hz during scattering produce wavefield with frequency of 7-20 Hz (Fig.5)). By using the SNRS algorithm, we select these scattered low-frequency waves and then analyze them.

Referee: Figure 11 (a), the 2D profile needs to be further tuned to avoid abrupt change in Vs.

Authors: We used only three 1D models to obtain the 2D model. We cannot smooth this model more.

Referee: Figure 12, the data quality of the real data is not good, even though it is acquired in a quiet environment. The green's function is really quite contaminated; therefore, the dispersion image is not clear. Nevertheless, understand the green's function is retrieved from the SNRS algorithm. It would be interesting to compare the green's function and dispersion image retrieved by conventional method. From there, readers would have a more explicit sense of the advantage of SNRS, if any.

Authors: It was the topic of our previous research and one of the reasons for development SNRS algorithm. As we showed earlier (Afonin et al., 2019), conventional methods of stacking EGFs in passive seismic interferometry are not working in the seismically quiet areas of Finland where industrial activity is practically absent and sources of seismic noise with high frequency (higher than 1 Hz) are rare, irregular and have low energy. In addition, high frequency noise from these sporadic sources attenuates rapidly and do not propagate to large distances. Therefore in our case, the signal and the dispersion curve presented in Figure 12, have relatively high quality. Conventional passive seismic interferometry not allowed evaluating EGF's.

Referee: Figure 13, there are some differences of the results from the proposed method and the conventional active method. Which one would be closer to real situation? A more discussion would be expected.

Authors: Figure 13 does not present results of comparison of models obtained by conventional analysis of surface waves from active sources (like MASW) with the model obtained by our method. Such comparison is not possible because vibrator does not produce Rayleigh waves of low frequencies (see Fig. 14, this is Fig. 15 in the revised manuscript). Figure 13 (Figure 14 in the revised manuscript) shows comparison of velocity models, obtained by analysis of wavefield produced by scattering of signal of vibrator (Fig. 13 (b)) with the wavefield produced by scattering of waves of unknown source (Fig. 13 (a)). That is why in our study we compared them not to each other, but to a priori geological information. Both of them do not contradict the geological information. From Figure 12 (b) one can see that the width of error bars of dispersion curves are about 500 m/s. Differences in velocities between two 2D models (Figure 13) are within these limits.

Referee: Same comments to Figure 12 applies for Figure 16. Figure 17, is it have an figure or table to validate or compare with the 2D profile with existing wells?

Authors: Unfortunately, there are too few data from wells in the studied area available for comparison.

The wells drilled by Geological Survey of Finland does not penetrate deep, and the data of wells drilled by exploration companies are not available for research organisations. We compared our results with geological information (boundaries of geological units) and with the data about rock properties and composition in XSoDEx area summarized by Leväniemi et al. (2018). In this study no direct measurements of S-wave velocities were made. The presented results are the first detailed information about shear wave seismic velocities in the subsurface for the studied area.

References

Afonin, N., Kozlovskaya, E., Nevalainen, J., Narkilahti, J.: Improving the quality of empirical Green's functions, obtained by cross-correlation of high-frequency ambient seismic noise, *Solid Earth*, 10(5), 1621-1634, <https://doi.org/10.5194/se-10-1621-2019>, 2019

Bohlen, T., Mueller, Ch. And Milkereit, B.: Elastic Seismic Wave Scattering from Massive Sulfide Orebodies. On the role of Composition and Shape. In: Eaton, D.W., Milkereit, B., and Salisbury, M. *Hardrock Seismic Exploration. Geophysical Developments No. 10*, Society of Exploration Geophysics, pp. 70-89, 2003.

Gritto, R., Korneev, V. A., & Johnson, L. R. (1995). Low-frequency elastic-wave scattering by an inclusion: limits of applications. *Geophysical Journal International*, 120(3), 677-692.

Leväniemi, H., Melamies, M., Mertanen, S., Heinonen, S., Karinen, T.: Petrophysical measurements to support interpretation of geophysical data in Sodankylä, northern Finland, Geological Survey of Finland Open File Work Report 25/2018, 2018

Mulargia, F. (2012). The seismic noise wavefield is not diffuse. *The Journal of the Acoustical Society of America*, 131(4), 2853-2858.

Wapenaar, K.: Retrieving the Elastodynamic Green's Function of an Arbitrary Inhomogeneous Medium by Cross Correlation, *Physical review letters*, 93(25), 254301, <https://link.aps.org/doi/10.1103/PhysRevLett.93.254301>, 2004

Author response to the interactive comment posted by Anonymous referee #2

First of all, we would like to point out that we use the old figure numbers in our replies. In the revised manuscript one new figure was added and numeration of figures has changed.

Referee: The authors present an application of passive seismic interferometry to image the subsurface of a mineral exploration area in northern Finland (down to 300 m). Passive seismic data were collected in parallel to active reflection/refraction acquisitions (during downtimes) along several linear profiles. The main purpose of the underlying project being active seismic experiments, only a short amount of continuous passive data could be collected (hours/days). The authors try to address the challenging task of retrieving meaningful surface-wave responses from such a short duration dataset. They claim that they could achieve this despite the non-stationary and non-isotropic distribution of noise sources. For that, they used an advanced processing algorithm called SNRS (not described in the work). They also claim (using supporting synthetic modeling) that this achievement was favored by strong local scattering conditions (local scattering helps reaching more diffuse field conditions). Using inversion of the extracted dispersion curves, they provide different 2D sections of shear-wave velocity models and propose some geological interpretations. While I agree that the topic and goals of this work are of high interest, I do not feel at this stage that the claims made by the authors are reliably backed up in the presented work, and I think that many points should be clarified.

My major concerns are the following:

- I do not understand how the numerical simulations address the problem of nonstationary/ non-isotropic noise sources. The position/angles of the sources have to be clarified, but it seems from the presented configurations that only the "pseudo-1D" case is tackled. By that I mean that the incoming noise horizontal direction seems to match the direction of the profile. This is a very favorable condition that does not address the main challenge of an off-angle dominant source of noise.

Authors: We considered different positions and types of sources (in line with the profile in surface (vibrator, waterpower plant dam and blast), sources out-of-line and also plane wave arriving with different incidence angles). Such positions were selected because in our study area we know positions of vibrator, dam and the active mine. In simulations we were just trying to represent situation with these real noise sources we identify in our experiment areas. In other experiments the sources may have different positions with respect to profiles, of course, but this is out of scope of our case-study paper. Moreover, when we considered a plane wave, which is an approximation of any source in far field area, we tested several incidence angles and azimuths of arrivals. In all cases, we noticed scattered arrivals with characteristics (polarization, dispersion) of Rayleigh waves and the similar apparent velocities for all considered cases. The similar scattered arrivals we noticed in synthetic seismograms, produced by vibrator, explosive source or dam located in-line with the profile. In the cases when the source was a plane wave or vibrator, we noticed that scattered arrivals have lower frequencies than the source, and that the scattered waves have polarization and apparent velocities typical for Rayleigh waves. Therefore, our modelling suggests that seismic waves from considered sources are converted to diffused wavefield of lower frequencies when scattering. Our modelling is in line with results of previous theoretical studies (for example, Gritto

et. al., 1995; Wapenaar, 2004). The analysis of real data recorded in XSoDEx project and presented in
715 our papers proves our suggestions.

Referee: As explained, the passive acquisition was made in parallel to active seismic acquisitions. This
is a great opportunity to make detailed comparisons of active vs passive data and benchmark noise
720 correlation/SNRS in a challenging configuration. One convincing comparison example was made for one
subsurface model (Figure 13). This approach could be generalized to compare: EGFs to "active" surface-
waves, dispersion curves, and other subsurface models. In my opinion, this would make a much more
compelling case for the passive approach than the numerical modeling invoked above.

Authors:
725 Direct comparison of the results from the proposed method and from the conventional methods based on
surface wave analysis from active sources (like MASW, for example) is impossible because vibrator does
not produce Rayleigh waves of low frequencies that we used in our method (Fig. 14). We pointed out on
this in the text of Section 3 and this was the main motivation for our synthetic modelling. Figure 13 shows
730 comparison of velocity models obtained by analysis of wavefield produced by scattering of signal from
vibrator (Fig. 13 (b)) with the model obtained using scattering of waves of unknown source (Fig. 13 (a)).
Therefore, in both cases, the scattering field is used and we applied our method in both cases in order to
obtain EGFs. That is why neither of the models can be considered as a benchmark. We compare both
models mainly to geological information and we find no contradiction. From Figure 12 (b) one can see
735 that the width of error bars of dispersion curves are about 500 m/s. Differences in velocities between two
2D models (Figure 13) are within these limits.

Referee: The title and paper stress-out the importance of using the advanced SNRS algorithm. However,
this algorithm is not described at all in the present work. Additionally, to ensure that SNRS is actually
740 required here, a comparison with traditional ambient noise correlation processing could be a great addition
(comparing EGFs with active data for example).

Authors: It was the topic of our previous research and one of the reasons for development SNRS
algorithm. The detailed description of the algorithm and results of its testing with real data in two different
areas with different type of ambient noise sources are already published in the paper by Afonin et al.
745 (2019). As we showed in this previous study, using of conventional passive seismic interferometry for
extracting empirical Green's functions from seismic noise of high frequency (higher than 1 Hz) is
practically impossible in seismically quiet areas of Finland where significant industrial activity is absent
and sources of seismic noise with high frequency are rare, irregular and have low energy. In addition,
high frequency noise from these sporadic sources attenuates rapidly and do not propagate to large
750 distances, so simple noise crosscorrelation does not work.
Concerning comparison with the active data, see our reply to the question above.

755 **Referee:** In the abstract, the passive dataset is said to contain only several hours of data. In the text, several days of acquisitions are mentioned. The exact record duration(s) should be mentioned as this is a key aspect of this work.

760 **Authors:** We used data intervals with durations varying from several hours to couple of days (it was the period when vibrator was in reparation). When we analyzed parts of records with vibrosource in Section 6 it was one day of continuous data. When we analyzed passive seismic data without vibrator, it was a couple of days. Nevertheless, we analyzed continuous seismic data without selecting parts of records with signal of vibrator. The SNRS method is selecting automatically parts of the record for retrieving EGFs.

765 **Referee:** The workflow from dispersion curves to subsurface models could be explained in more details.

Authors: The main steps of data processing are described in Section 5. They are well known (MASW for obtaining dispersion curves, inversion of dispersion curves using Geopsy). References and a new figure (Figure 10) describing the workflow is added to the text.

770 **Referee:** Why not comparing the resulting models with the results of the main project (reflection/refraction models)?

775 **Authors:** To the moment, detailed models from analysis of reflected and refracted P-waves are still not published in regular papers. That is why we decided not to include any preliminary results of these studies into our paper that concentrates mainly on analysis of S-wave velocities down to 300 m. We compared our results mainly with petrophysical and geological information.

780 **Referee:** The matching or lack of matching between model and boundary of geological units is not clearly discussed (Fig. 17).

Authors: The XSoDEx study is the first one, where upper subsurface of this area was studied in such details. Our study reveals boundaries between major lithological units in the area. However, it is necessary to take into account that the boundaries of geological units in this area are known with certain precision, depending on density of points for geological sampling. That is why certain discrepancy between previously defined boundaries of geological units and geophysical information is possible. Geologists need input from geophysical studies in order to upgrade their knowledge.

Referee: The quality of the figures should be improved, as well as the quality of the language.

790 **Authors:** The quality of the figures has been improved and we made additional work on language.

Referee: Some detailed comments are provided in the attached annotated pdf. Please also note the supplement to this comment: <https://se.copernicus.org/preprints/se-2020-160/se-2020-160-RC2-supplement.pdf>

795

Authors: Replies to these comment provided in attached.

References

800 Afonin, N., Kozlovskaya, E., Nevalainen, J., Narkilahti, J.: Improving the quality of empirical Green's
functions, obtained by cross-correlation of high-frequency ambient seismic noise, *Solid Earth*, 10(5),
1621-1634, <https://doi.org/10.5194/se-10-1621-2019>, 2019.
Bohlen, T., Mueller, Ch. And Milkereit, B.: Elastic Seismic Wave Scattering from Massive Sulfide
805 Orebodies. On the role of Composition and Shape. In: Eaton, D.W., Milkereit, B., and Salisbury, M.
Hardrock Seismic Exploration. Geophysical Developments No. 10, Society of Exploration Geophysics,
pp. 70-89, 2003.
Gritto, R., Korneev, V. A., & Johnson, L. R. (1995). Low-frequency elastic-wave scattering by an
inclusion: limits of applications. *Geophysical Journal International*, 120(3), 677-692.
Wapenaar, K.: Retrieving the Elastodynamic Green's Function of an Arbitrary Inhomogeneous Medium
810 by Cross Correlation, *Physical review letters*, 93(25), 254301,
<https://link.aps.org/doi/10.1103/PhysRevLett.93.254301>, 2004